Atmospheric Research 260 (2021) 105688

Contents lists available at ScienceDirect

Atmospheric Research

journal homepage: www.elsevier.com/locate/atmosres

Distinguishing features of high altitude negative leaders as observed with LOFAR

O. Scholten [a,b,c,*], B.M. Hare [a,*], J. Dwyer [d], N. Liu [d], C. Sterpka [d], S. Buitink [e,f], A. Corstanje [e,f], H. Falcke [e,g,h,i], T. Huege [j,f], J.R. Hörandel [e,f,g], G.K. Krampah [f], P. Mitra [f], K. Mulrey [f], A. Nelles [k,l], H. Pandya [f], J.P. Rachen [f], T.N.G. Trinh [m], S. ter Veen [h], S. Thoudam [n], T. Winchen [f]

[a] University Groningen, Kapteyn Astronomical Institute, Landleven 12, 9747, AD, Groningen, the Netherlands
[b] University of Groningen, KVI Center for Advanced Radiation Technology, Groningen, the Netherlands
[c] Interuniversity Institute for High-Energy, Vrije Universiteit Brussel, Pleinlaan 2, 1050 Brussels, Belgium
[d] Department of Physics and Space Science Center (EOS), University of New Hampshire, Durham, NH 03824, USA
[e] Department of Astrophysics/IMAPP, Radboud University Nijmegen, Nijmegen, the Netherlands
[f] Astrophysical Institute, Vrije Universiteit Brussel, Pleinlaan 2, 1050 Brussels, Belgium
[g] Nikhef, Science Park Amsterdam, Amsterdam, The Netherlands
[h] Netherlands Institute for Radio Astronomy (ASTRON), Dwingeloo, the Netherlands
[i] Max-Planck-Institut für Radioastronomie, Auf dem Hügel 69, 53121 Bonn, Germany
[j] Institute for Astroparticle Physics, Karlsruhe Institute of Technology(KIT), P.O. Box 3640, 76021 Karlsruhe, Germany
[k] Erlangen Center for Astroparticle Physics, Friedrich-Alexander-Univeristät Erlangen-Nürnberg, Germany
[l] DESY, Platanenallee 6, 15738 Zeuthen, Germany
[m] Department of Physics, School of Education, Can Tho University Campus II, 3/2 Street, Ninh Kieu District, Can Tho City, Viet Nam
[n] Department of Physics, Khalifa University, PO Box 127788, Abu Dhabi, United Arab Emirates

ARTICLE INFO

Keywords:
Thunderstorms
Lightning
Radio emission
Negative leaders
Corona flash
LOFAR lightning imaging

ABSTRACT

We present high resolution observations of negative leaders at high altitude using the LOFAR radio telescope. We show that the structure of negative leaders at high altitude (altitudes larger than 7 km) differs in several respects from that of negative leaders at lower altitudes. In particular, the High Altitude Negative Leaders (HANLs) show very distinct steps of a few hundred meters, stepping times of the order of a few milliseconds and a filamentary structure that extends outward over several hundreds of meters; as opposed to lower altitude ($\lesssim$ 5 km) leaders, which have stepping times and distances around 0.01 ms and 10 m. Similar to lower altitude leaders, high altitude leaders emit copious VHF radiation from their propagating tip and have propagation velocities of the order of 10^5 m/s. Corona-flash like bursts can be distinguished when zooming in to meter and nanosecond scales.

1. Introduction

Lightning is a well known process that, however, harbors much poorly understood physics. Being an electric phenomenon, a lightning discharge proceeds with positively and negatively charged channels in the atmosphere, called leaders, that are rather hot and reasonably conducting (Dwyer and Uman, 2014; da Silva et al., 2019). It is well known from early streak camera observations that positive leaders propagate (or grow) in a rather continuous fashion while the negative leaders, which are the prime subject of this work, usually propagate in discrete jumps, called steps (Dwyer and Uman, 2014). The physics picture behind this observed stepping process in lightning is still not clear because detailed in-situ observations are difficult.

It has been observed that the structure of lightning stepping depends on the altitude, and thus on air pressure. (Wu et al., 2015) reported that the stepped leaders propagate faster at lower altitudes. At lower altitudes (Lyu et al., 2016) finds a stepping length that seems much larger than what has been found in (Hare et al., 2019). This may be related to the better resolving power of the observations presented in (Hare et al., 2019). In addition (Lyu et al., 2016) as well as (Wu et al., 2015) focussed their work on the initial part of the leaders in contrast to (Hare et al., 2019) where the leaders after the initial stage were considered.

Using the Dutch stations of LOFAR, it has become possible to make high resolution (in space and time) images of lightning flashes using

* Corresponding authors at: University Groningen, Kapteyn Astronomical Institute, Landleven 12, 9747, AD, Groningen, the Netherlands.
E-mail addresses: O.Scholten@rug.nl (O. Scholten), B.H.Hare@rug.nl (B.M. Hare).

https://doi.org/10.1016/j.atmosres.2021.105688
Received 19 January 2021; Received in revised form 18 May 2021; Accepted 19 May 2021
Available online 26 May 2021

radio waves (in the 30–80 MHz band) for which clouds are transparent. In this work we report on observations of High Altitude Negative Leaders (HANL) that show a structure that is markedly different from negative leaders at lower altitudes. We present an initial survey of the structure of the HANL, which we recognize in all negative leaders at altitudes in excess of 7 km. They distinguish themselves from normal, lower altitude, negative leaders by a very dense envelope of a long (sometimes 300 m) filamentary structure. In addition, probably related to the lengths of the filaments, we observe a stepping length that is an order of magnitude longer than that for lower altitude negative leaders. Since the stepping time is an order of magnitude larger too, the propagation speed is very similar to that of negative leaders at lower altitudes (which we label as 'normal'). The long stepping length combined with the resolution that can be achieved with LOFAR allows us to resolve the fine detailed dynamics of this stepping process in natural lightning. It is Interesting to note that (Lyu et al., 2016) observed similar stepping lengths and times for higher altitude leaders as are found in this work.

Long streamer structures on negative leaders have been observed before. In (Edens et al., 2014) photographic images are shown of such a high altitude negative leader as it exits a cloud. These observation show rather long and dense clusters of streamers that appear to be very similar to what we have observed in radio.

Most of the flashes we have observed with LOFAR ((Hare et al., 2019; Scholten et al., 2021a; Hare et al., 2020; Scholten et al., 2021b)) show initiation at a height of 4–5 km with positive leaders at higher altitudes (up to about 8 km) and negative leaders below. In three flashes (out of over 20 that were analyzed) we observe negative leaders at altitudes above 7 km and all (six in total) show very similar features.

2. Methods

Our Lightning imaging procedure uses the time-traces recorded with LOFAR (van Haarlem et al., 2013), a radio telescope primarily used for astronomy, that combines the signals in the frequency range from 10 to 240 MHz from thousands of antennas distributed over a large part of Europe. For this work we limit ourselves to the Dutch portion of this telescope that contains the core and remote stations up to 70 km from the core, see Appendix A and use the 30–80 MHz band.

A lightning flash is imaged by locating the sources that emit VHF-pulses. From the (interferometric) cross-correlations between small sections of the time-traces for different antennas with that for a reference antenna, we obtain arrival time differences for a pulse from the same VHF-source. From these arrival time differences for 100–400 antennas we 'locate' the position and time of the impulsive point source by triangulation. The total of all these sources make the 4D (space & time) image of the flash (see (Scholten et al., 2021a) for a more in-depth discussion of the procedure). Since we search for the maxima in the cross correlations between the signals in antenna pairs one may also regard our procedure for locating the sources as finding the most likely position (in 3D) of the interferometric maximum for a short (100 ns long) section of the time trace containing impulsive emission from a VHF-source.

The basic technique of determining arrival time differences from the cross correlation of signals in different antennas is used rather broadly for systems with a small (less than 10) number of antennas and baselines of the order of hundreds of meters, see (Rhodes et al., 1994; Shao et al., 1995; Kawasaki et al., 2000; Dong et al., 2001; Qiu et al., 2009; Yoshida et al., 2010; Akita et al., 2010; Sun et al., 2013; Akita et al., 2014; Stock et al., 2014; Liu et al., 2018). With LOFAR, we typically use a few hundreds of antennas and baselines of up to 100 km. This allows us to reach the unprecedented accuracy of a few meters in VHF imaging (Hare et al., 2020; Scholten et al., 2021a).

3. Analysis

We observed that negative leaders at high altitudes have a structure that differs considerably from that of normal negative leaders observed at low altitude (Hare et al., 2020). Scanning through all our fully imaged flashes we found such a structure in only three from a total of more than twenty imaged flashes, and these negative leaders all occurred an altitudes higher than 7 km. No normal negative leaders have been observed at these altitudes. We therefore name them High Altitude Negative Leaders (HANLs), although it should be noted that the compelling evidence is not a proof that the observed features are indeed directly linked to the altitude of the leaders. The three flashes were recorded on September 21, 2018 at 19:42:59 UTC (Flash A, showing 1 HANL) and two on August 14, 2020, Flash B at 14:14:58 UTC (showing 3 HANLs) and Flash C at 14:32:41 UTC (also showing 3 HANLs). In this work we focus on flashes A and B. Flash C shows similar features. The complete images for each of these three flashes is given in Appendix A. The weather map for flash A can be seen at (KNMI, 2018) and that for the 2020 flashes at (KNMI, 2020).

A typical example of such a HANL is shown in Fig. 1, where it is compared to a negative leader seen in the same flash (Flash B) at a lower altitude. It is immediately clear that they are rather different. Compared to normal negative leaders we observe at lower altitudes, typically below 6 km, HANLs.

- have a much larger lateral spread, of the order of 100 m or more while normal negative leaders show a lateral spread of the order of 10 m.
- have a much larger number of sources per unit length, in Fig. 1, for example, there are 6443 sources on the left and only 1787 on the right.
- show a 'feathery' substructure formed by a large number of long filaments.
- show propagation in large steps in space (order of a few 100 m) and time (a few milliseconds, see also Fig. 2) as compared to steps of less than 10 m in 0.05 ms intervals for normal negative leaders (Hare et al., 2020) observed with LOFAR.

The sub-structure seen in a HANL is elaborated upon in the following section while in Section 3.2 the transition from a normal negative leader to a HANL is discussed.

HANLs have some properties that are very similar to those of normal negative leaders that distinguishes them from positive leaders or dart leaders such as:

- impulsive activity at the propagating tip only, as opposed to positive leaders that show impulsive VHF emission in twinkles along most of their length (Hare et al., 2019).
- propagate at typical speeds of order 10^5 m/s as opposed to recoil leaders that propagate one order of magnitude faster.
- have a conductive core that is (sometimes) made visible by recoil leaders.

Most of these properties are immediately clear from Fig. 1. The HANL covers a distance of 3 km in 60 ms and thus propagates with 0.5×10^5 m/s while the right shows a recoil leader propagating with 0.6×10^6 m/s followed at $t = 220$ ms by a negative leader propagating at 0.7×10^5 m/s. This speed is typical for all HANLs we have observed. The recoil leader passed through a channel that supported earlier recoil leaders at $t = 70$ ms and at $t = 150$ ms as seen in Fig. A.7, left.

We observe recoil leaders passing through a HANL, sometimes more than once, often about 100 ms after the HANL was formed. The large HANL seen in Flash C continues to propagate at the tip after a quiet period at about $t = 100$ ms, see right side of Fig. A.7. These properties are not unlike one may find in normal negative leaders.

3.1. Structure of a HANL

Already in Fig. 1 one may distinguish that the 'fuzzy' structure of a

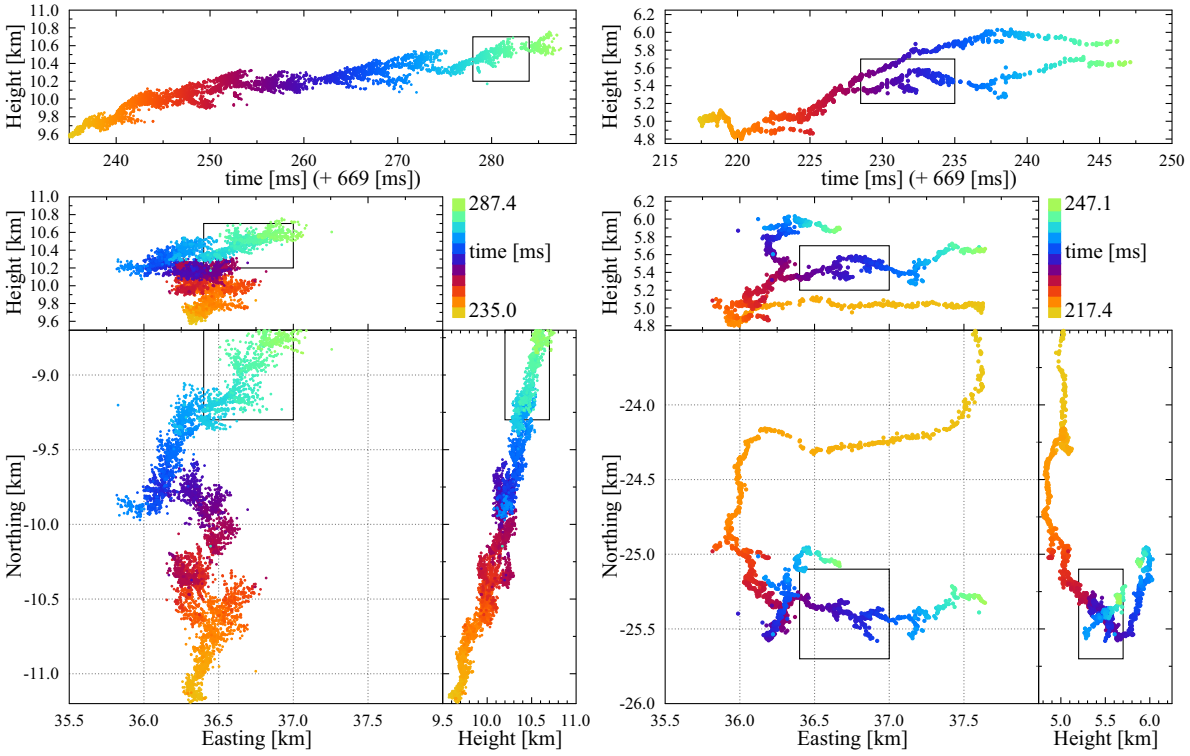

Fig. 1. Comparing the images of a HANL (from Flash B) with that of a lower altitude negative leader from the same flash, occurring at similar times (as seen from the top panels), but different altitudes and Northing positions. The initial part of the negative leader on the right, till about $t = 220$ ms, is a recoil leader and the rest a stepped leader. The same length scales are used in both images. The boxes indicate the zoomed-in volumes for Fig. 2.

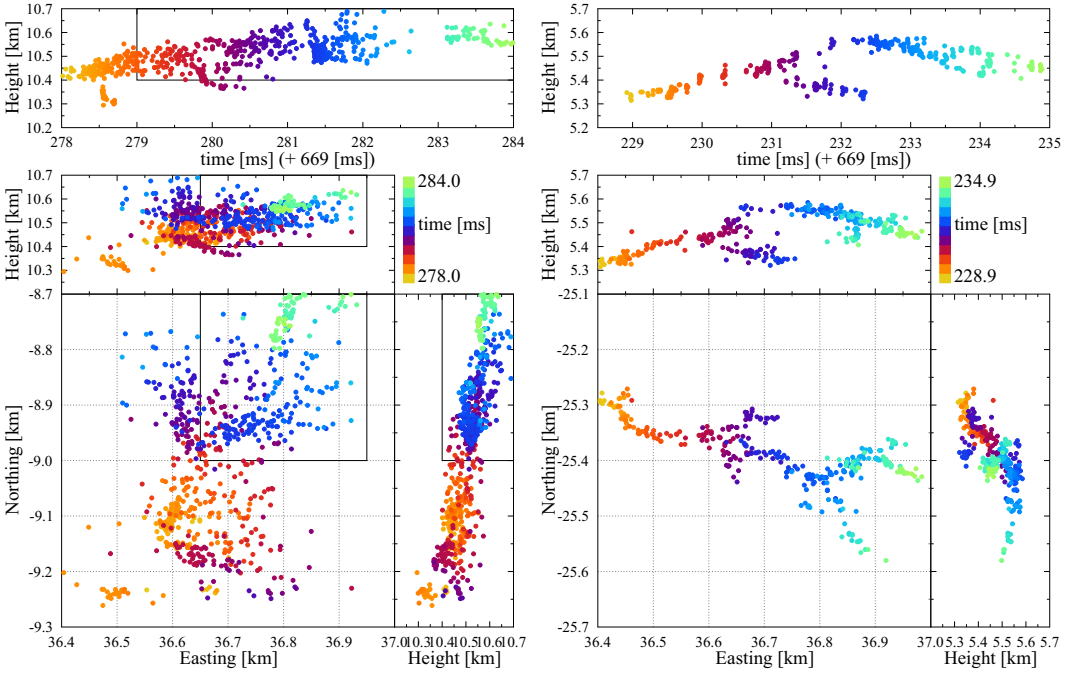

Fig. 2. The left side shows a zoom-in on the HANL of Fig. 1 showing the filamentary structure while the right a zoom-in on a normal negative leader in the same flash. Both sides use the same scales. The box on the right indicates the zoomed-in volume for Fig. 3.

HANL is in fact formed by a filamentary structure pointing outward at an angle of approximately 45° with respect to the main backbone structure. A zoom-in on this structure is presented on the left of Fig. 2 showing several filaments fanning out from a common origin, in sharp contrast with the structure of a normal negative leader shown on the right. The filaments may be streamers or leaders or something in between, but since we cannot distinguish them at this stage we prefer the more neutral label of filaments. A HANL appears to consist of a core surrounded by a rather dense filamentary structure, where each filament may reach a length of 300 m, although for Flash A these filaments are shorter and

reach 100 m at most. Our VHF mapping does not reveal the core of the structure, and so its location can only be derived from later recoil leaders.

Propagation of the HANL is by a sequence of steps where each step consists of a large number of filaments fanning-out from a common center. At the end of the reach of these filaments the process may repeat itself. Each step may cover a distance of a few 100 m with several milliseconds between steps. This can be seen from the plan view presented in Fig. 2. Since the steps are this large and clearly visible in the images, there was no need to perform a statistical analysis of the stepping length like what was done in (Hare et al., 2020).

To investigate the dynamics of one such a step and its filamentary nature we show in Fig. 3 a further zoom in on the HANL-section displayed in Fig. 2. To show the dynamics of this structure we show a sequence of frames covering small (but unequal) time-steps.

Frame 1; 279.0–281.25 ms In the first frame the previously formed filaments from a burst occurring at [(N,E,h) = (−9.12, 36.58, 10.4) km and t = 278.3 ms, see Fig. 2] keep developing and streaming outward seemingly unaffected at an average speed of 1.1 × 10^5 m/s. This frame shows two, possibly three, filaments that appear to fork.

Frame 2; 281.25–281.5 ms In the second frame a burst is triggered (indicated by the red circle in the plan view) showing a copious number of VHF-sources, while at the same time VHF-sources show as a semicircle in the plan view at the tips of the filaments seen in the earlier frame. The burst starts at t = 281.35 ms at a position where filaments were seen in the previous frame much earlier at t = 279.58 ms. Initially this burst develops very rapidly, covering 100 m in 0.15 ms after which it slows down to about 3 × 10^5 m/s as can be seen in the next frame.

Frame 3; 281.5–282.0 ms The burst from the first frame keeps on expanding. Again a filamentary structure can be seen, although we reach the limit of our imaging capability.

Frame 4; 282–284 ms The last frame shows two more bursts starting at t = 283.1 ms, almost simultaneously some 100 m apart, and a third one at t = 283.6 ms (all three indicated by red circles in the plan view). The height v.s. Northing suggest that the burst of frame two did not (yet) pass through this area, and thus they seem all three to be triggered by the burst from the first frame, 1–2 ms after the ionization front passed through this area. The features seen here are typical for all HANLs.

Optical observations of lightning (Dwyer and Uman, 2014, Fig. 4.1) show that during the step formation, the leader brightens and extends in length while producing a burst of streamers at its tip, called a corona flash. Because optical measurements are sensitive to hot channels, the corona flash, composed of cold streamer filaments, is usually poorly resolved in optical. In electric field change observations of negative leader stepping (Krider et al., 1977), where one is sensitive to the electric currents, the intensity is maximal at the time and position of the flash, then rapidly decreasing, followed by a quiet period until the next flash. Even though in VHF observations are less sensitive to currents along the channel but very sensitive to streamers activity the picture is completely consistent with our earlier VHF observations of negative leaders (Hare et al., 2020). Also in Fig. 3 the intensity (as can be read from the density of sources) is strongly increasing at the time of the flash followed by a near exponential decrease with a quiet period before the next flash. A possible interpretation might be thus be that the bursts we see in Fig. 3 are corona flashes with outgoing streamers which we see as filaments. Even though this picture may be tempting, it is surprising to observe such a small number of streamers that even extend as far as a few 100 m from their starting point. From the images shown in Fig. 3 it can be seen that these filaments tend to branch. The filaments do emit VHF pulses which are a signature of currents that vary at nanosecond scales (Shi et al., 2016). Thus observing VHF emission can be the indication that we are dealing with branching negative streamers.

If these filaments are instead gradually growing streamers it is not understood what causes the emission of short (~50 ns long) VHF-pulses. This thus might indicate that the streamers do not grow gradually but more in an erratic pattern, even though generally in the direction of the ambient field.

An open issue is what the physics is that determines the position of the next corona flash. Since they appear to occur at the outer reach of the filaments from the previous flash it seems unlikely that this is position is determined by the crossing of multiple streamers (Biagi et al., 2010; Dwyer and Uman, 2014). It seems more likely that at this site there happened to be a larger size hydrometeor or that this is the tip of a filament when it stopped propagating. Since we do not see any evidence of a growing space stem, neither of a space stem connecting to the old leader tip at the time of the next corona flash, it seems more likely that charge starts to accumulate through the (poorly conducting) streamer body until there is a sufficient amount to create a corona burst (Briels et al., 2008; Kochkin et al., 2014, 2015; Celestin et al., 2015). The observed fact that this appears to happen at the outer reach of the filament structure could be explained by assuming that in the region covered by the filaments the conductivity is large enough that any point will not be able to accumulate charge, charge accumulation can only occur at the outer perimeter of the ionized region. While it is tempting to identify the present VHF observations of HANLs with negative leader stepping, we should be cautious because at present we do not have simultaneous optical and VHF measurements and it is not clear if HANLs are indeed just larger versions of normal leader steps.

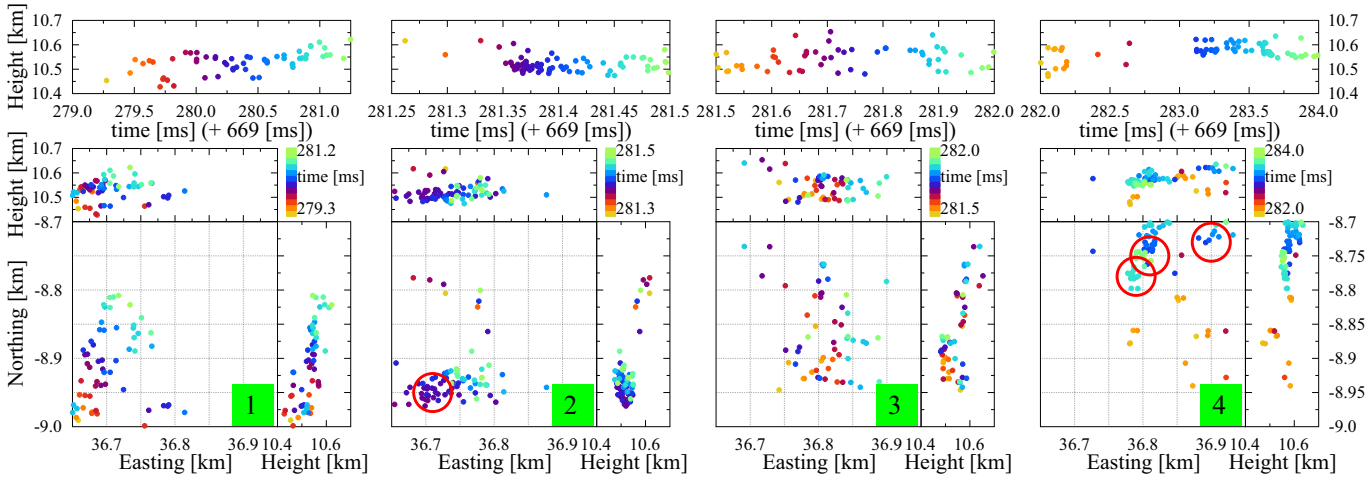

Fig. 3. Slow motion 'movie', with unequal time-frames, for a zoom-in on the HANL shown in Fig. 2. The emerging bursts are marked with a red circle in Frames 2 and 4.

It may also be that the filaments are small leaders. In this case the VHF sources probably mark the steps in these negative leaders. However in this case the long wait between the passing of the leader and the following corona flash is difficult to explain.

3.2. Abrupt change of leader structure

Most of the HANLs we observed started already at rather high altitude, since the earlier part of these flashes were not recorded, and show all properties of a HANL already from the onset. An exception is the upgoing negative leader seen in Flash A (see Fig. A.6 in Appendix A for an overview). This leader started at a mere 4 km height to propagate almost straight up to level off at an altitude of 8 km. This upward going negative leader in Flash A starts out as a rather typical normal negative leader with fast and short steps and a lateral spread of about 10 m but shows the properties of a HANL when propagating at 8 km height. Since the leader is propagating upward in a rather curvy path (see Appendix B) it is difficult to discern its properties in a usual image and instead we show in Fig. 4 the statistics of the spread of the VHF sources around the mean path.

To emphasize the change in structure of the leader while propagating upward, we show in Fig. 4 the distribution of the distances of the sources with respect to the leader-core, drawn in light-blue in Fig. B.9. The red part of Fig. 4 applies to the leader at 4.6–6.0 km altitude while blue refers to the leader when it has reached 6.6–7.8 km altitude. Unfortunately, there are two negative leaders propagating upward in close proximity between 6.0 and 6.6 km altitude, see Fig. B.8, making the assignment of VHF-sources to one or the other leader ambiguous and for this reason this section could not be displayed. The scatter plots show the distance of the VHF-source location to the head of the propagating leader as function of time while the leader is propagating mostly upward. The histogram shows the probability distribution for the source distance for the two leader sections separately; red (long dashed) for the lower and blue (short dashed) for the higher altitudes.

The statistics marked in red in Fig. 4 is typical for a normal negative leader. The lateral spread is of the order of 10 m and individual steps are too close to distinguish on this scale (as shown in (Hare et al., 2020) the stepping time for a normal negative leader is of the order of 0.1 ms) thus the points spread rather homogeneously in time. The right side shows a considerably larger spread in distance to the leader, however still much smaller than what the HANL depicted in Fig. 1 shows. Another typical feature of a HANL is that the sources come in millisecond bursts. This burst structure is also clearly visible in the scatter panel. The structure of the negative leader thus has changed considerably over 5 milliseconds after climbing only one kilometer. The fact that the signature of a HANL is not as outspoken as for the example shown in Fig. 1 is probably because the HANL structure is more strongly developed at larger heights.

The trend of increasing stepping time and increasing stepping length may already have been observed in (Lyu et al., 2016) where for altitudes in excess of 9 km, a stepping length of 300 m and stepping times of the order of 1.5 ms are reported, which is similar to what we observe for the HANLs.

4. Summary and discussion

At high altitudes we observed that the structure of negative leaders is very different from that of negative leaders at lower altitudes. The structure changes at a rather well defined altitude (between 5.5 and 6.5 km). The most noteworthy distinctions are the dense filamentary structure of the HANL and the bunched structure, where the bunches are separated by about one filament length, that can be on the order of 300 m at the highest altitudes. Since these leaders propagate at about the same velocity as normal negative leaders, these bunches occur once every few millisecond. It is not certain if these filaments are in fact streamers or leaders or something in between. We find the HANL structure for all our negative leaders at an altitude above 7 km, with no exception, and thus we assume that the structure and the altitude are linked, although for a hard proof more statistics on HANLs would be required. The fact that long stepping time and distances were also observed in (Lyu et al., 2016) for negative leaders at the highest altitudes, we see as additional circumstantial evidence.

In general one expects that with increasing height and thus decreasing pressure the properties of a discharge gradually change. A dependence of leader properties on altitude was observed already in (Wu et al., 2015). The present observations suggest that there is a critical height at which the structure changes rather abruptly. At an altitude of 7 km, at a pressure of about 500 mbar, the length of streamers appears to vary strongly with pressure and one, in fact, reaches some kind of phase transition. It is not understood why very impulsive VHF emission occurs during the propagation of the filaments.

According to similarity laws for streamers, the streamer transverse size scales inversely proportional with gas density (Liu and Pasko, 2004; Nijdam et al., 2020). However, to form very long streamers that take a long time to grow, the three body attachment, which leads to a loss of electrons and decrease of conductivity in the channel, is important. Because three-body attachment scales are inversely proportional to the square of the density, this mechanism will become quickly less

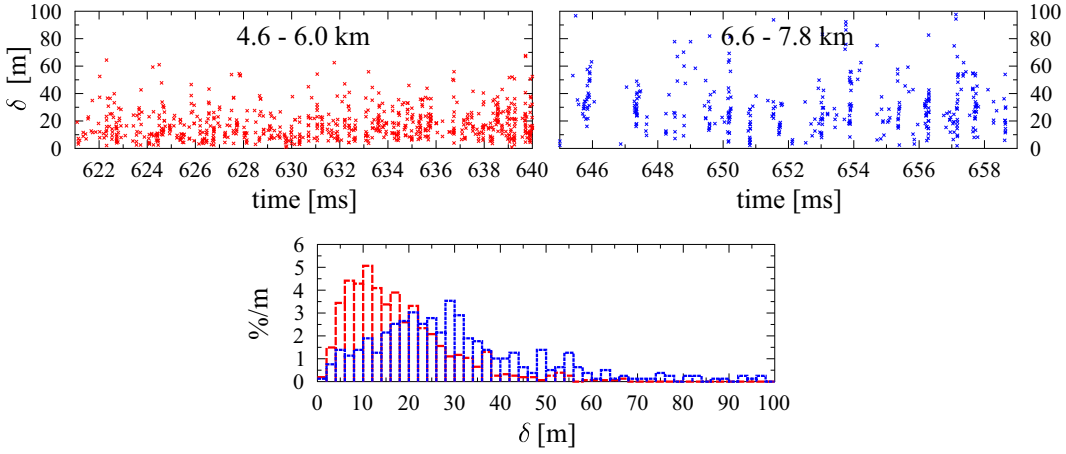

Fig. 4. Statistics for two section of Flash A, right before (red) and after (blue) from where a negative leader transitions from normal to a HANL. In red the distance of the VHF sources to the mean leader head position, δ, is shown for the part of the leader between 4.6 and 6.0 km altitude and in blue for the 6.6–7.8 km altitude range while the leader is mostly propagating upward.

important with increasing density. This thus favors a more than proportional increase of streamer length with altitude. The size of the streamer corona, which is generally the size of the region over which the average field is equal to the streamer propagation threshold field, is by itself also inversely proportional to the air density. Combining these effects, the streamer corona length could thus increases very rapidly with altitude.

Following the above argumentation it may be that the structure of low and high altitude negative leaders is in fact not different at all and one is dealing only with a non linear rapid increase of the streamer length at a certain pressure. It might thus be that the physics of HANL stepping is the same as that of normal negative leader stepping, but only on a much expanded scale. If so, HANLs offer the unique possibility to observe for natural lightning, using the LOFAR imaging capability, the fine-structure of the negative leader stepping process.

Credit author statement

O. Scholten: wrote the original draft of the manuscript and carried the main data analysis.

B. M. Hare: contributed much to the methodology and was strongly involved in all aspects that led to the completion of the work.

J. Dwyer, N. Liu, andC. Sterpka were involved in the analysis of the data and the main physics ideas.

As members of the LOFAR cosmic ray key science project the following authors played a role in the acquisition of LOFAR data:

S. Buitink, A. Corstanje, H. Falcke, B. M. Hare, T. Huege, J. R. Hörandel, G. K. Krampah, P. Mitra, K. Mulrey, A. Nelles, H. Pandya, J. P. Rachen, O. Scholten, T. N. G. Trinh, S. ter Veen, S. Thoudam, T. Winchen

Declaration of Competing Interest

The authors declare that they have no known competing financial interests or personal relationships that could have appeared to influence the work reported in this paper.

Acknowledgements

The LOFAR cosmic ray key science project acknowledges funding from an Advanced Grant of the European Research Council (FP/2007-2013) [ERC grant number 227610]; The project has also received funding from the European Research Council (ERC) under the European Union's Horizon 2020 research and innovation programme [grant number 640130]; BMH is supported by the NWO [grant number VI.VENI.192.071]; AN is supported by the DFG [grant number NE 2031/2-1]; TW is supported by DFG [grant number 4946/1-1]; KM is supported by FWO [grant number FWOTM944]; TNGT acknowledges funding from the Vietnam National Foundation for Science and Technology Development (NAFOSTED) under [Grant number 103.01-2019.378]; ST acknowledges funding from the Khalifa University Startup grant [project code 8474000237];

This paper is based on data obtained with the International LOFAR Telescope (ILT). LOFAR (van Haarlem et al., 2013) is the Low Frequency Array designed and constructed by ASTRON. It has observing, data processing, and data storage facilities in several countries, that are owned by various parties (each with their own funding sources), and that are collectively operated by the ILT foundation under a joint scientific policy. The ILT resources have benefitted from the following recent major funding sources: CNRS-INSU, Observatoire de Paris and Université d'Orléans, France; BMBF, MIWF-NRW, MPG, Germany; Science Foundation Ireland (SFI), Department of Business, Enterprise and Innovation (DBEI), Ireland; NWO, The Netherlands; The Science and Technology Facilities Council, UK.

Appendix A. Overview of the three flashes with HANLs

An overview of each of the three flashes discussed in this work and where HANLs are observed is given in Fig. A.6, Fig. A.7. See (KNMI, 2018) and (KNMI, 2020) for the weather maps for the time periods around those of Flash A and B and C. It should be noted that for Thunderstorms in the LOFAR area the charge layers are usually lying at lower altitudes (Trinh et al., 2020) than generally seen in tropical and subtropical storms.

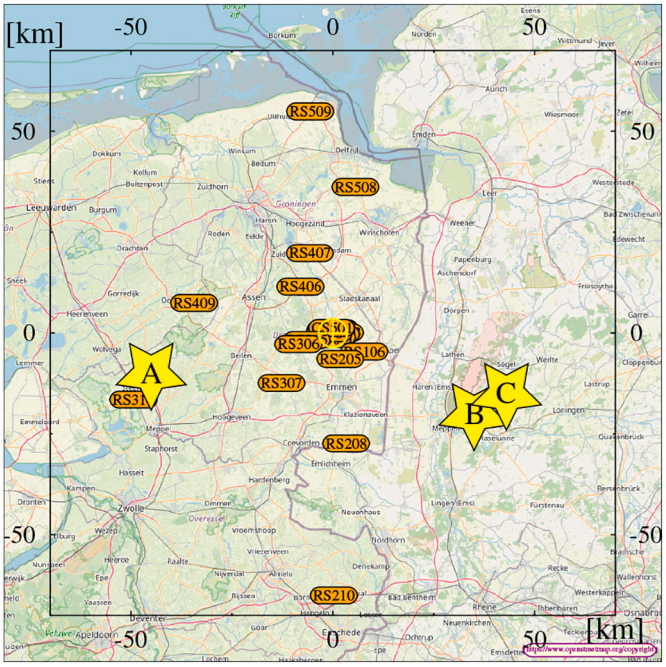

Fig. A.5. Layout of the Dutch LOFAR stations. The core of LOFAR is indicated by the yellow $\oplus$ sign while the yellow stars show the general location of flashes A, B, and C that are discussed in this work. The black frame indicates the general area (140×140 km^2) w here flashes can be mapped accurately. (For interpretation of the references to colour in this figure legend, the reader is referred to the web version of this article.)

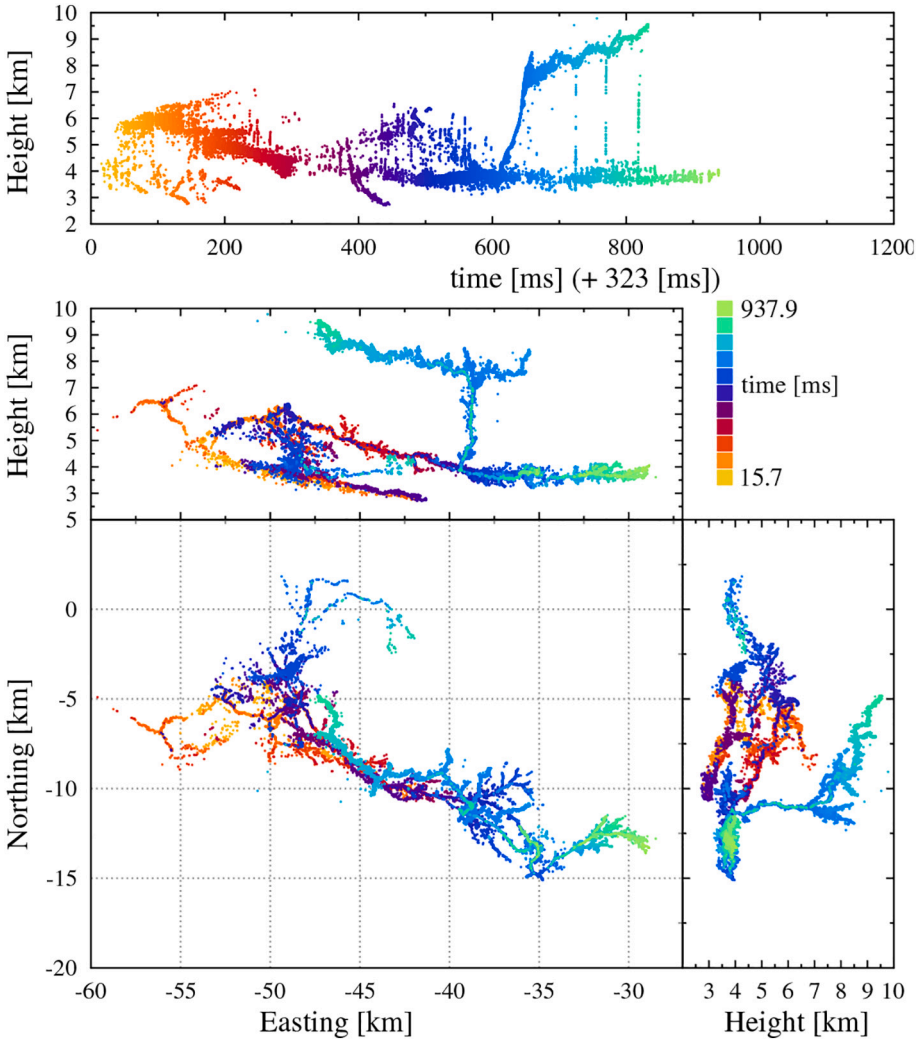

Fig. A.6. Overview of Flash A. The weather map for the time of this flash can be retrieved from (KNMI, 2018).

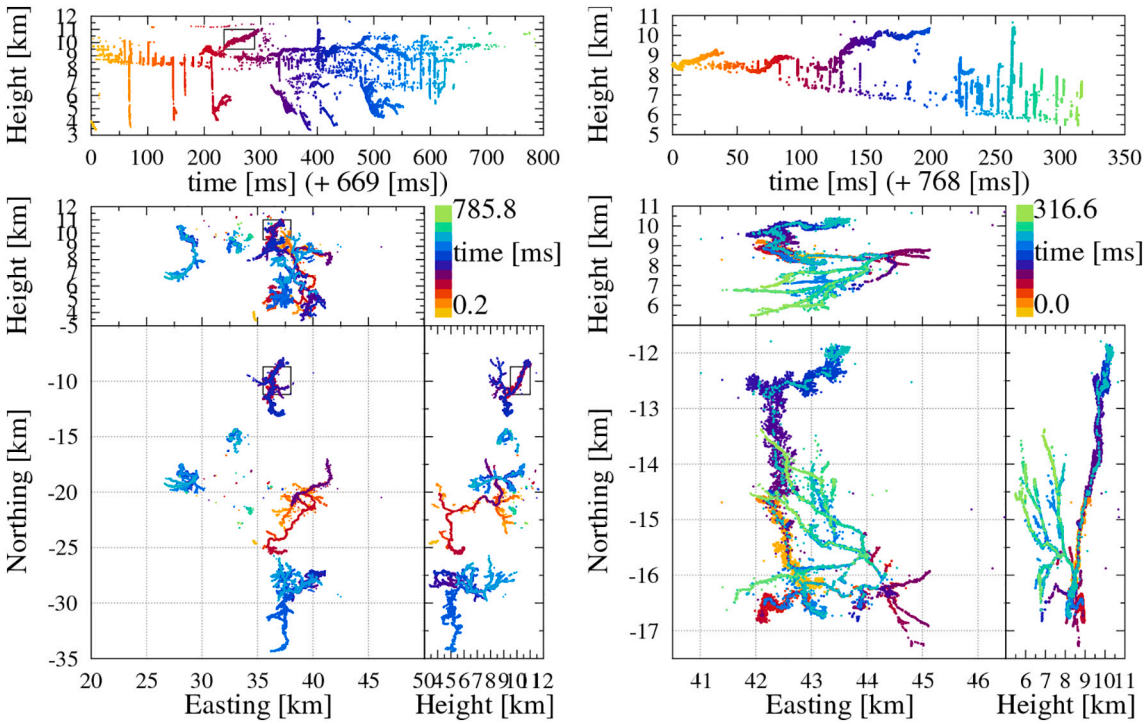

Fig. A.7. Overview of the two 2020 flashes that show a HANL, Flash B and C. The zoom-in on the larger HANL of Flash B is shown in Fig. 1. The weather map for the time of these flash can be retrieved from (KNMI, 2020).

Appendix B. Upward leader section in Flash A

The upward negative leader of Flash A is shown in Fig. B.8. This leader starts out as a normal negative leader at an altitude of 4.5 km and converts to a HANL on its way up. Two zoom-ins of the leader are shown in Fig. B.9, left when it is still a normal negative leader and right when it just was converted into a HANL. However, due to the upward propagation the HANL and the limited altitude of the leader, its properties do not show as prominently as for the HANL shown in Fig. 1. To emphasize the differences in structure the statistics of the distances of VHF sources to the mean leader position, indicated by the light-blue line in Fig. B.9, is shown in Fig. 4.

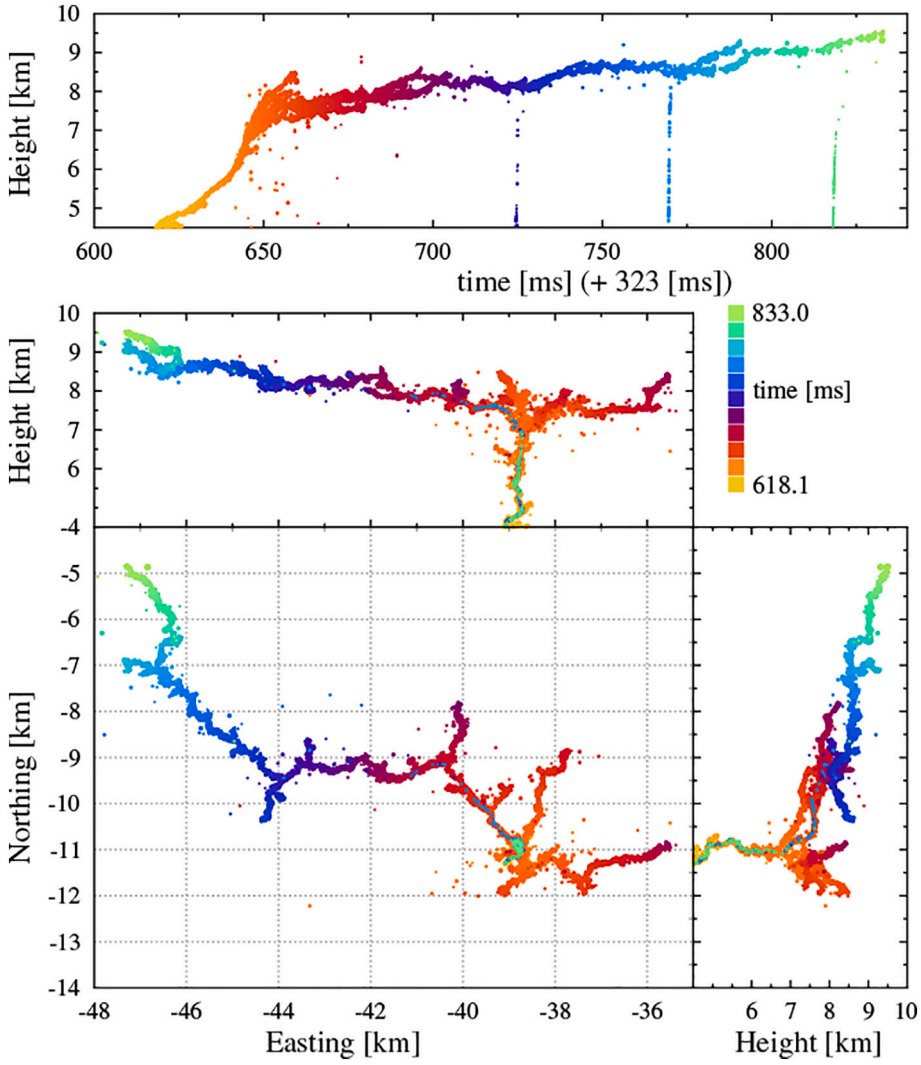

Fig. B.8. The upward leader of Flash A (see Fig. A.6).

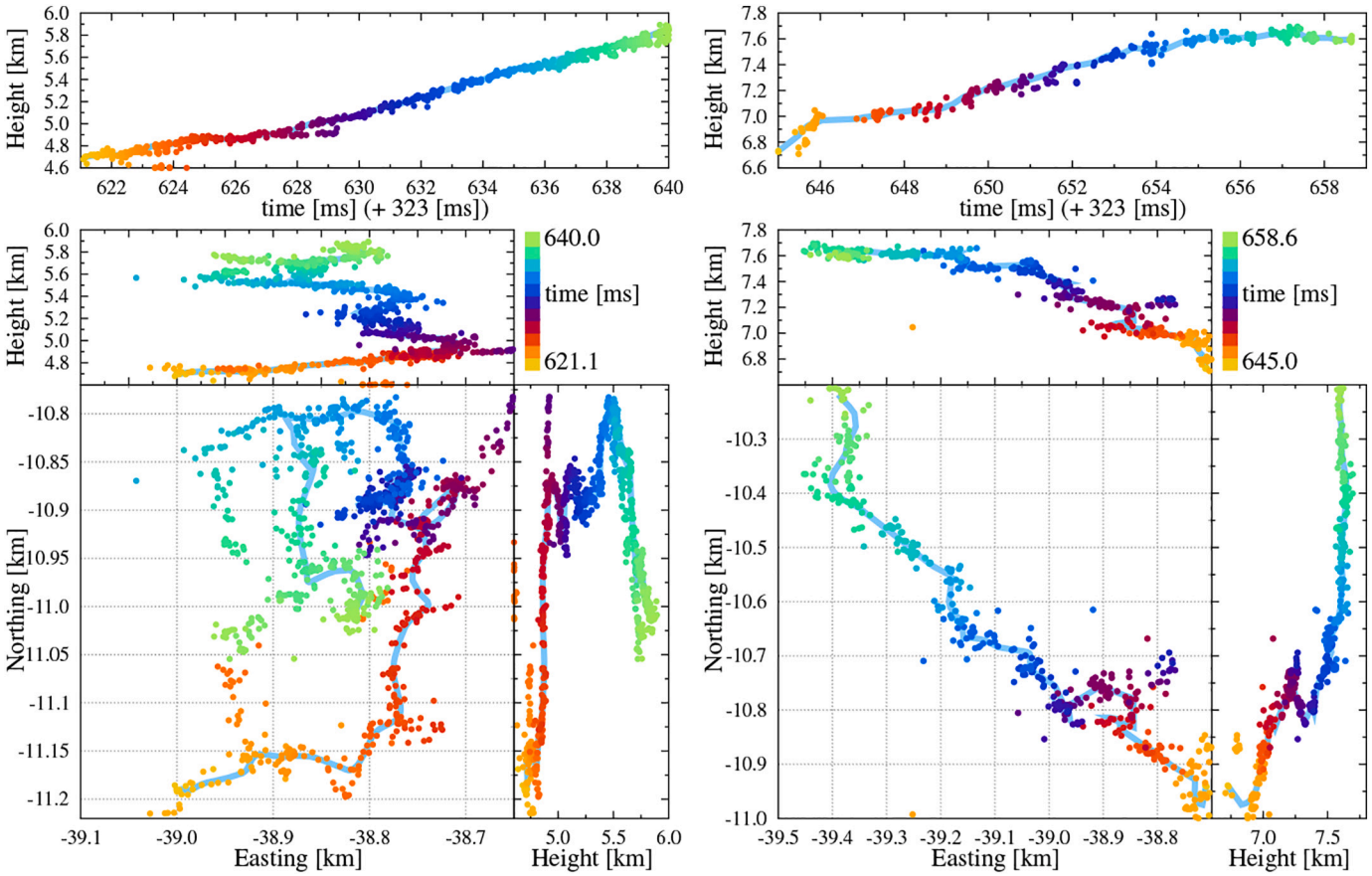

Fig. B.9. The sections of the upward leader of Flash A, shown in Fig. B.8 that are used to extract the systematics of the deviation of the sources from the average leader position, shown by the light-blue band, that is shown in Fig. 4. (For interpretation of the references to colour in this figure legend, the reader is referred to the web version of this article.)

Appendix C. Data statement

The data are available from the LOFAR Long Term Archive (for access see (ASTRON, 2020)). To download this data, please create an account and follow the instructions for "Staging Transient Buffer Board data" at (ASTRON, 2020). In particular, the utility "wget" should be used as follows:

wget https://lofar-download.grid.surfsara.nl/lofigrid/SRMFifoGet.py?surl="location" where "location" should be specified as:

srm://srm.grid.sara.nl/pnfs/grid.sara.nl/data/lofar/ops/TBB/lightning/ followed by

L668464_D20180921T194259.023Z_"stat"_R000_tbb.h5 (for Flash A)

L792864_D20200814T143241.768Z_"stat"_R000_tbb.h5 (for Flash B)

`L792864_D20200814T143241.768Z_"stat"_R000_tbb.h5` (for Flash C) and where "stat" should be replaced by the name of the station, CS001, CS002, CS003, CS004, CS005, CS006, CS007, CS011, CS013, CS017, CS021, CS024, CS026, CS028, CS030, CS031, CS032, CS101, CS103, RS106, CS201, RS205, RS208, RS210, CS301, CS302, RS305, RS306, RS307, RS310, CS401, RS406, RS407, RS409, CS501, RS503, RS508, or RS509.

The processed data used for making Figs. 1–4 is available at (Scholten et al., 2021c).

All figures in this work have been made using the Graphics Layout Engine (GLE) Pugmire et al. (2015) plotting package.

References

Akita, M., Nakamura, Y., Yoshida, S., Morimoto, T., Ushio, T., Kawasaki, Z., Wang, D., 2010. What occurs in k process of cloud flashes? J. Geophys. Res.-Atmos. 115 https://doi.org/10.1029/2009JD012016.

Akita, M., Stock, M., Kawasaki, Z., Krehbiel, P., Rison, W., Stanley, M., 2014. Data processing procedure using distribution of slopes of phase differences for broadband VHF interferometer. J. Geophys. Res.-Atmos. 119, 6085–6104. https://doi.org/10.1002/2013JD020378.

ASTRON, 2020. LOFAR Long Term Archive Access. https://www.astron.nl/lofarwiki/doku.php?id=public:lta_howto.

Biagi, C.J., Uman, M.A., Hill, J.D., Jordan, D.M., Rakov, V.A., Dwyer, J., 2010. Observations of stepping mechanisms in a rocket-and-wire triggered lightning flash. J. Geophys. Res.-Atmos. 115. URL: https://agupubs.onlinelibrary.wiley.com/doi/abs/10.1029/2010JD014616, doi: doi:10.1029/2010JD014616, arXiv:https://agupubs.onlinelibrary.wiley.com/doi/pdf/10.1029/2010JD014616.

Briels, T.M.P., van Veldhuizen, E.M., Ebert, U., 2008. Time resolved measurements of streamer inception in air. IEEE Trans. Plasma Sci. 36, 908–909. https://doi.org/10.1109/TPS.2008.920223.

Celestin, S., Xu, W., Pasko, V.P., 2015. Variability in fluence and spectrum of high-energy photon bursts produced by lightning leaders. J. Geophys. Res. Space Physics 120, 10712–10723. URL: https://hal-insu.archives-ouvertes.fr/insu-01351316. https://doi.org/10.1002/2015JA021410.

da Silva, C.L., Sonnenfeld, R.G., Edens, H.E., Krehbiel, P.R., Quick, M.G., Koshak, W.J., 2019. The plasma nature of lightning channels and the resulting nonlinear resistance. J. Geophys. Res.-Atmos. 124, 9442–9463. URL: https://agupubs.onlinelibrary.wiley.com/doi/abs/10.1029/2019JD030693, doi: doi:10.1029/2019JD030693, arXiv:https://agupubs.onlinelibrary.wiley.com/doi/pdf/10.1029/2019JD030693.

Dong, W., Liu, X., Yu, Y., Zhang, Y., 2001. Broadband interferometer observations of a triggered lightning. Chin. Sci. Bull. 46, 1561–1565. https://doi.org/10.1007/BF02900582.

Dwyer, J.R., Uman, M.A., 2014. The physics of lightning. Phys. Rep. 534, 147–241. https://doi.org/10.1016/j.physrep.2013.09.004 the Physics of Lightning.

Edens, H.E., Eack, K.B., Rison, W., Hunyady, S.J., 2014. Photographic observations of streamers and steps in a cloud-to-air negative leader. Geophys. Res. Lett. 41, 1336–1342. https://doi.org/10.1002/2013GL059180.

Hare, B.M., et al., 2019. Needle-like structures discovered on positively charged lightning branches. Nature 568, 360–363. https://doi.org/10.1038/s41586-019-1086-6.

Hare, B.M., Scholten, O., Dwyer, J., Ebert, U., Nijdam, S., Bonardi, A., Buitink, S., Corstanje, A., Falcke, H., Huege, T., Hörandel, J.R., Krampah, G.K., Mitra, P., Mulrey, K., Neijzen, B., Nelles, A., Pandya, H., Rachen, J.P., Rossetto, L., Trinh, T.N. G., ter Veen, S., Winchen, T., 2020. Radio emission reveals inner meter-scale structure of negative lightning leader steps. Phys. Rev. Lett. 124, 105101. URL: https://link.aps.org/doi/10.1103/PhysRevLett.124.105101, doi: 10.1103/PhysRevLett.124.105101.

Kawasaki, Z., Mardiana, R., Ushio, T., 2000. Broadband and narrowband rf interferometers for lightning observations. Geophys. Res. Lett. 27, 3189–3192. https://doi.org/10.1029/1999GL011058.

KNMI, 2018. Weather Map for Flash A. https://tinyurl.com/2bw629mz.

KNMI, 2020. Weather Map for Flash B. https://tinyurl.com/y466aaww.

Kochkin, P., van Deursen, A., Ebert, U., 2014. Experimental study of the spatio-temporal development of metre-scale negative discharge in air. J. Phys. D. Appl. Phys. 47, 145203. https://doi.org/10.1088/0022-3727/47/14/145203.

Kochkin, P.O., van Deursen, A.P.J., Ebert, U., 2015. Experimental study on hard x-rays emitted from metre-scale negative discharges in air. J. Phys. D. Appl. Phys. 48, 025205. URL: doi:10.1088%2F0022-3727%2F48%2F2%2F025205. https://doi.org/10.1088/0022-3727/48/2/025205.

Krider, E.P., Weidman, C.D., Noggle, R.C., 1977. The electric fields produced by lightning stepped leaders. J. Geophys. Res. 82 (1896–1977), 951–960. URL: https://agupubs.onlinelibrary.wiley.com/doi/abs/10.1029/JC082i006p00951, doi: doi:10.1029/JC082i006p00951, arXiv:https://agupubs.onlinelibrary.wiley.com/doi/pdf/10.1029/JC082i006p00951.

Liu, N., Pasko, V.P., 2004. Effects of photoionization on propagation and branching of positive and negative streamers in sprites. J. Geophys. Res. Space Physics 109. URL: https://agupubs.onlinelibrary.wiley.com/doi/abs/10.1029/2003JA010064, doi: doi:10.1029/2003JA010064, arXiv:https://agupubs.onlinelibrary.wiley.com/doi/pdf/10.1029/2003JA010064.

Liu, H., Qiu, S., Dong, W., 2018. The three-dimensional locating of vhf broadband lightning interferometers. Atmosphere 9. URL: https://www.mdpi.com/2073-4433/9/8/317, doi: 10.3390/atmos9080317.

Lyu, F., Cummer, S.A., Lu, G., Zhou, X., Weinert, J., 2016. Imaging lightning intracloud initial stepped leaders by low-frequency interferometric lightning mapping array. Geophys. Res. Lett. 43, 5516–5523. https://doi.org/10.1002/2016GL069267.

Nijdam, S., Teunissen, J., Ebert, U., 2020. The physics of streamer discharge phenomena. Plasma Sources Sci. Technol. 29, 103001. URL: doi:10.1088/1361-6595/abaa05, doi: 10.1088/1361-6595/abaa05.

Pugmire, C., Mundt, S.M., LaBella, V.P., Struyf, J., 2015. Graphics Layout Engine gle 4.2.5 User Manual https://en.wikipedia.org/wiki/Graphics_Layout_Engine. URL: https://glx.sourceforge.io/index.html, arXiv:http://www.gle-graphics.org/.

Qiu, S., Zhou, B.H., Shi, L.H., Dong, W.S., Zhang, Y.J., Gao, T.C., 2009. An improved method for broadband interferometric lightning location using wavelet transforms. J. Geophys. Res.-Atmos. 114. https://doi.org/10.1029/2008JD011655.

Rhodes, C.T., Shao, X.M., Krehbiel, P.R., Thomas, R.J., Hayenga, C.O., 1994. Observations of lightning phenomena using radio interferometry. J. Geophys. Res.-Atmos. 99, 13059–13082. https://doi.org/10.1029/94JD00318.

Scholten, O., Hare, B.M., Dwyer, J., Sterpka, C., Kolmasova, I., Santolik, O., Lan, R., Uhlir, L., Buitink, S., Corstanje, A., Falcke, H., Huege, T., Hoerandel, J.R., Krampah, G.K., Mitra, P., Mulrey, K., Nelles, A., Pandya, H., Pel, A., Rachen, J.P., Trinh, T.N.G., Veen, S.t., Thoudam, S., Winchen, T., 2021a. The initial stage of cloud lightning imaged in high-resolution. J. Geophys. Res.-Atmos. 126, e2020JD033126. URL: https://agupubs.onlinelibrary.wiley.com/doi/abs/10.1029/2020JD033126, doi: doi:10.1029/2020JD033126. e2020JD033126 2020JD033126.

Scholten, O., et al., 2021b. A distinct negative leader propagation mode. Submitted Sci. Rep. https://doi.org/10.21203/rs.3.rs-402945/v1.

Scholten, O., et al., 2021c. Processed Data for "Distinguishing Features of High Altitude Negative Leaders as Observed with LOFAR" https://doi.org/10.34894/MGLPXM.

Shao, X.M., Krehbiel, P.R., Thomas, R.J., Rison, W., 1995. Radio interferometric observations of cloud-to-ground lightning phenomena in Florida. J. Geophys. Res.-Atmos. 100, 2749–2783. https://doi.org/10.1029/94JD01943.

Shi, F., Liu, N., Rassoul, H.K., 2016. Properties of relatively long streamers initiated from an isolated hydrometeor. J. Geophys. Res.-Atmos. 121, 7284–7295. URL: https://agupubs.onlinelibrary.wiley.com/doi/abs/10.1002/2015JD024580, doi: doi:10.1002/2015JD024580, arXiv:https://agupubs.onlinelibrary.wiley.com/doi/pdf/10.1002/2015JD024580.

Stock, M.G., Akita, M., Krehbiel, P.R., Rison, W., Edens, H.E., Kawasaki, Z., Stanley, M. A., 2014. Continuous broadband digital interferometry of lightning using a generalized cross-correlation algorithm. J. Geophys. Res.-Atmos. 119, 3134–3165. https://doi.org/10.1002/2013JD020217.

Sun, Z., Qie, X., Liu, M., Cao, D., Wang, D., 2013. Lightning VHF radiation location system based on short-baseline TDOA technique; Validation in rocket-triggered lightning. Atmos. Res. 129-130, 58–66. https://doi.org/10.1016/j.atmosres.2012.11.010.

Trinh, T.N.G., Scholten, O., Buitink, S., Ebert, U., Hare, B.M., Krehbiel, P.R., Leijnse, H., Bonardi, A., Corstanje, A., Falcke, H., Huege, T., Hörandel, J.R., Krampah, G.K., Mitra, P., Mulrey, K., Nelles, A., Pandya, H., Rachen, J.P., Rossetto, L., Rutjes, C., ter Veen, S., Winchen, T., 2020. Determining electric fields in thunderclouds with the radiotelescope LOFAR. J. Geophys. Res.-Atmos. 125, e2019JD031433. URL: https://agupubs.onlinelibrary.wiley.com/doi/abs/10.1029/2019JD031433, doi: 10.1029/2019JD031433. e2019JD031433 10.1029/2019JD031433.

van Haarlem, M.P., et al., 2013. LOFAR: the LOw-Frequency ARray. A&A 556, A2. https://doi.org/10.1051/0004-6361/201220873.

Wu, T., Yoshida, S., Akiyama, Y., Stock, M., Ushio, T., Kawasaki, Z., 2015. Preliminary breakdown of intracloud lightning: initiation altitude, propagation speed, pulse train characteristics, and step length estimation. J. Geophys. Res.-Atmos. 120, 9071–9086. URL: https://agupubs.onlinelibrary.wiley.com/doi/abs/10.1002/2015JD023546, doi: doi:10.1002/2015JD023546, arXiv:https://agupubs.onlinelibrary.wiley.com/doi/pdf/10.1002/2015JD023546.

Yoshida, S., Biagi, C.J., Rakov, V.A., Hill, J.D., Stapleton, M.V., Jordan, D.M., Uman, M. A., Morimoto, T., Ushio, T., Kawasaki, Z.I., 2010. Three-dimensional imaging of upward positive leaders in triggered lightning using vhf broadband digital interferometers. Geophys. Res. Lett. 37. https://doi.org/10.1029/2009GL042065.